

Motion of a particle near a rough wall in a viscous shear flow

By F. CHARRU¹, E. LARRIEU¹, J.-B. DUPONT¹
AND R. ZENIT²

¹Institut de Mécanique des Fluides de Toulouse - UMR CNRS/INPT/UPS 5502,
2, Avenue Camille Soula, 31400 Toulouse, France

²Instituto de Investigaciones en Materiales, Universidad Nacional Autónoma de
México, México D.F. 04510, México

(Received 20 October 2005 and in revised form 9 June 2006)

The motion of a spherical particle along a rough bed in a simple shear viscous flow is studied experimentally for a wide range of parameters, varying the particle size and density, the fluid viscosity and the shear rate γ . The instantaneous particle velocity is calculated in the stream, transverse and vertical directions, using a high-speed video imaging system. It is found that the normalized streamwise mean particle velocity U/U_S , where U_S is the Stokes settling velocity, depends only on the dimensionless shear rate $\mu\gamma/(\Delta\rho gd)$, this relationship being independent of the particle Reynolds number Re_p . This result holds for small Re_p , which was the case in our experiments ($Re_p < 10$). The characteristic amplitude and frequency of the velocity fluctuations are also given and discussed. A model is then proposed for the mean streamwise velocity, based on ideas of Bagnold (*Proc. R. Soc. Lond. A*, vol. 332, 1973, p. 473) and calculations of Goldman *et al.* (*Chem. Engng Sci.*, vol. 22, 1967*b*, p. 653) for the velocity of a particle close to a smooth plane. From this model an equivalent bed roughness and an effective friction coefficient are deduced.

1. Introduction

The problem of the motion of a particle on a rough bed is of practical interest, such as in the cleaning of surfaces, filtration, field-flow fractionation, and is also relevant to the understanding of sediment transport and avalanches. For a particle falling down an inclined plane, two types of experiments have been reported, differing in the roughness size and the role of the surrounding fluid. In the first type, results have been reported on the fall of a particle in the ambient air down an inclined bed of fixed beads similar to the moving one (Riguidei *et al.* 1994; Quartier *et al.* 2000). In the second, a particle falling on small roughnesses in a viscous fluid has been studied by Zhao, Galvin & Davis (2002). The case considered here, when the driving force on the particle is imposed by a shearing flow and the roughness is of the same order of magnitude as the particle diameter, has received less attention.

The motion of a spherical particle near a smooth wall in a viscous shear flow, as sketched in figure 1(*a*), was investigated first by Goldman, Cox & Brenner (1967*a, b*), in the limit of zero inertia. These authors obtained the translating and rotating velocities of the free particle as functions of the shear rate γ , the particle radius a , and the distance h of the particle from the wall. More details will be discussed in §4. Small inertia effects were taken into account by Cherukat & McLaughlin (1994) who calculated the resulting lift force normal to the wall. King & Leighton

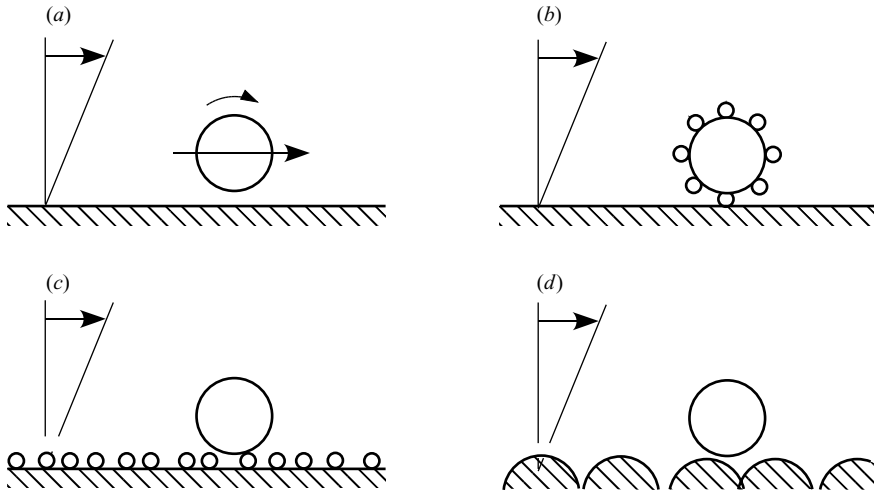


FIGURE 1. Sketch of the situations considered: (a) smooth particle near a smooth wall; (b) rough particle near a smooth wall; (c) smooth particle near a rough wall; (d) smooth particle near a particle bed.

(1997) and Krishnan & Leighton (1995) obtained the lift force for the limit when the sphere is in contact with the wall, and used this result to investigate the motion of a rough heavy sphere rolling on a horizontal smooth plane. In their model, sketched in figure 1(b), the centre of the sphere is maintained at a distance h from the wall by a typical roughness $(h - a) \ll a$. The calculated particle velocity was found to be in agreement with their experiments, with reasonable values of the roughness and friction coefficient.

The case of a smooth particle moving on a rough bed made of loosely packed fixed particles with diameter $(h - a)$ small compared to a , as sketched in figure 1(c), does not seem to have been considered until now. However, since the far-field flow differs from the previous case by a small amount of order $\gamma(h - a)$, it may be expected that the particle velocity can be obtained by the model of King & Leighton and Krishnan & Leighton with accuracy of order $(h - a)/a$.

The situation considered here is that of a particle moving on a bed of particles of the same diameter, as sketched in figure 1(d). This situation differs from the previous smooth case in several aspects: (i) the ‘roughness length’ $(h - a)$ is no longer well-defined, (ii) the up-and-down motion of the particle induces a mean slip velocity even if the particle rolls without sliding at the contact point, (iii) the particle moves only if the shear rate exceeds a threshold shear rate. These features significantly complicate theoretical analysis, and only a few experimental results are available. Francis (1973) and Abbot & Francis (1977) report mean particle velocities for turbulent flow, and a general theoretical framework was proposed by Bagnold (1973), as discussed in §4; yet no experimental results available for the case of viscous flow. This paper examines this case. Experiments are first reported for the motion of a particle over a bed of fixed particles with the same diameter; then a model is proposed to account for the mean velocity of a free particle, based on the concepts of equivalent roughness and effective friction coefficient. The experimental setup is described in §2, and the results are given in §3 for the particle motion: mean velocity and fluctuating motion in the three directions. A model is proposed in §4, and the final Section discusses the results.

Series	ρ (kg m ⁻³)	μ (mPa s)	H (mm)	ρ_p (kg m ⁻³)	d (mm)	U_s (mm s ⁻¹)	Re_p	θ	Symbol
1	976	113	8	2480	1.62	19.0	2.2	0.46	○
2	976	53	8	2480	1.62	40.6	2.8	0.13	◇
3	976	22	8	2480	1.62	97.8	8.3	0.066	▽
4	976	53	8	1140	1.59	4.26	1.7	0.76	△
5	976	50	9	1280	1.05	3.65	0.39	0.29	□

TABLE 1. Fluid and bead properties, Stokes settling velocity U_s , maximum values of the particle Reynolds number Re_p and Shields number θ , and corresponding symbol in figures.

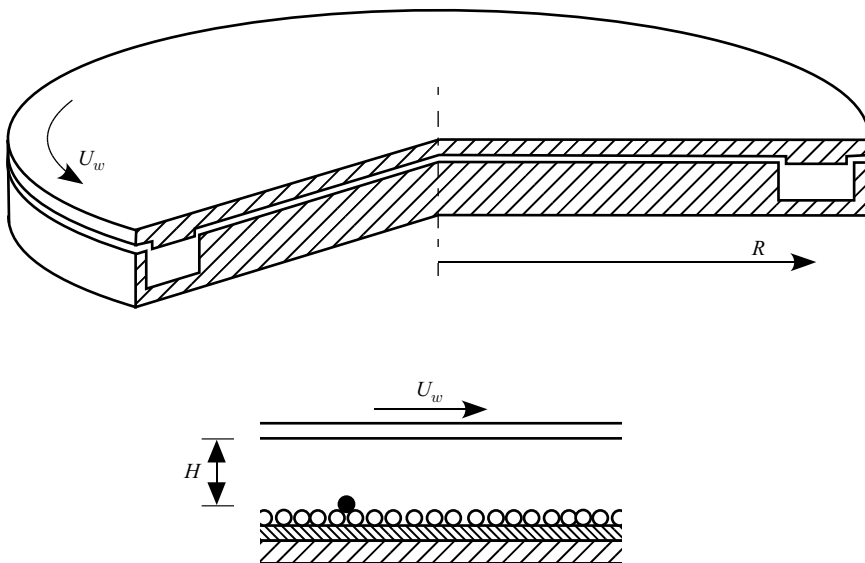


FIGURE 2. (a) Sketch of the annular channel with mean radius $R=200$ mm, channel width 40 mm and channel depth 20 mm. (b) Side view showing the annular ring on which the fixed particles are glued, and the moving particle. The fluid thickness H was in the range 8–9 mm.

2. Experimental setup

The experiments were carried out in an annular Plexiglas channel of rectangular cross-section, as shown in figure 2(a), with mean radius of 200 mm, and width and depth of 40 and 20 mm, respectively. The rough bed consisted of a monolayer of particles, glued on an annular ring set in the channel as shown in the side view in figure 2(b). The fluid thickness H , defined as the distance from the top of the glued particles to the upper plate, was in the range 8–9 mm, depending on the particle diameter (see table 1). Particles were nearly spherical and with nearly uniform diameter, the size dispersion being about $\pm 7\%$ of the mean diameter. They were glued randomly on the ring, a typical bed obtained in such a way being shown in figure 3, with a packing fraction of 0.77 ± 0.02 . Due to the small dispersion of particle size and the two-dimensional pattern, some crystallized areas could not be avoided.

The rotation of the upper plate, with velocity U_w at the mean radius R , drags the fluid, which in turn sets into motion the free particle deposited on the rough bed. In

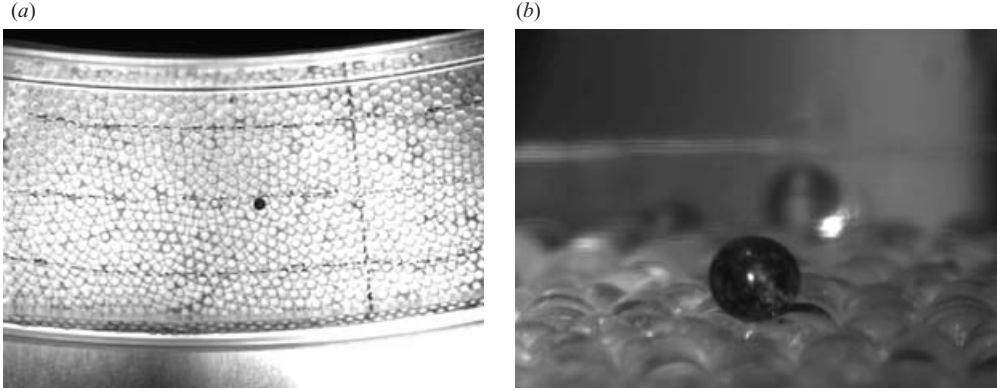


FIGURE 3. (a) Top view of the channel and particle bed; the black circle in the middle of the channel is the moving particle. (b) Side view of the moving particle on the bed.

the middle half of the channel, the dominant fluid motion is azimuthal, with uniform shear rate close to

$$\gamma = \frac{U_w}{H}. \quad (2.1)$$

Due to centrifugal effects, a secondary flow takes place, directed outwards close to the moving plate and inwards near the bed, which slowly drags the free particle towards the inner lateral wall of the channel. This secondary flow and its effect on the motion of particles have been described in detail in Charru, Mouilleron-Arnould & Eiff (2004), where the inertial correction of the shear rate (2.1) was given. For the experiments presented here, the shear Reynolds number

$$Re = \frac{\rho U_w H}{\mu}, \quad (2.2)$$

where ρ and μ are the fluid density and viscosity, was lower than 50 for most measurements, so that the inertial correction to the shear rate (2.1) was negligible.

The fluid and beads were chosen in order to vary the three main parameters: the density difference of the particle and fluid, $\rho_p - \rho$, the fluid viscosity, μ , and the particle diameter, $d = 2a$. The diameter of the moving particle is equal to that of the bed particles for all experiments. The five different sets of physical properties used are given in table 1. Series 1, 2 and 3 correspond to glass beads and three different fluid viscosities, series 4 corresponds to a Nylon bead with lower density, and series 5 to an acetate bead of smaller diameter.† In all series, the fluid is silicon oil. Also reported in table 1 is the Stokes settling velocity

$$U_S = \frac{(\rho_p - \rho) g d^2}{18 \mu}, \quad (2.3)$$

as well as the maximum values of the particle Reynolds and Shields numbers, defined as

$$Re_p = \frac{\rho \gamma d^2}{\mu} = \frac{d^2}{H^2} Re, \quad \theta = \frac{\mu \gamma}{(\rho_p - \rho) g d}. \quad (2.4)$$

† Glass beads were from Cultura, Loisirs et Décoration, Portet-sur-Garonne, France. Nylon beads were from Goodfellow, <http://www.goodfellow.com>, and acetate beads from Marteau & Lemarie, <http://www.marteau-lemarie.fr>.

It can be seen that the maximum values of the particle Reynolds number are smaller or slightly larger than one; hence, the effect of fluid inertia on the particle motion, as well as particle inertia, are expected to be small.

For series 1, the horizontal motion of the particle was recorded from above with a high-speed camera (250 and 500 frames per second) and a typical field of view of 30 particle diameters, corresponding to spatial resolution ranging from 33.8 to 46.3 pixels mm^{-1} . The vertical motion was also observed from the side view for a few runs. For series 2 to 5, only the horizontal motion of the particle was recorded and with a low-speed camera (20 to 60 frames per second), with a larger field of view corresponding to a spatial resolution in the range 11.6 to 12.4 pixels mm^{-1} . The centre of the moving particle was obtained from the digitized images, using a routine from the Matlab[®] image processing toolbox. To enhance the contrast of the images, the background was first subtracted. Then the image was converted into a binary image choosing an appropriate threshold level. The position of the centroid of the particle was then easily obtained with subpixel accuracy. The same procedure was applied to the entire image series; hence, the particle position (x, y, z) was obtained as a function of time, where x, y and z are the streamwise, transverse (directed outwards) and vertical (directed upwards) coordinates. Attempts have been made to measure rotational velocities by tracking tiny eccentric bubbles embedded in the particle; however due to the rotation in the three directions, these measurements had to be abandoned.

3. Results

3.1. Onset of motion

At rest, the particle typically is in contact with three bed particles, its bottom lying slightly below the plane tangent to the top of the particle bed. In order to move the particle out of its gravity potential well, a minimum non-zero shear rate is required, for which the moment of the hydrodynamic force at the pivoting point, of order $\mu\gamma d^2$, balances that of the immersed weight, of order $(\rho_p - \rho)gd^3$. This threshold shear rate defines a threshold Shields number θ_{t0} which depends on the height of the barrier potential to be overcome, i.e. on the initial position of the particle on the bed. Note that if both the surfaces of the moving and fixed particles were smooth, the particle touching the bed would not move in finite time; thus some roughness is needed, as discussed in §4 in relation to the theoretical model.

The threshold θ_{t0} was found to be in the range 0.02–0.04. For Shields number slightly above the threshold θ_{t0} , the particle was observed to travel a finite distance and eventually to stop. This stopping is likely to correspond to a fall into a deeper crevice or to contact with a larger bed particle preventing any further motion. For a given shear and a given initial position, the distance travelled by the particle was found to depend on the details of its trajectory, and exhibited large scatter. However, upon averaging, a mean value L of this distance appeared to be reached after about ten runs. The variation of this distance with Shields number, normalized with the particle diameter, is shown in figure 4 in linear and logarithmic scales. The distance appears to increase with the Shields number, as expected, and diverges for Shields number close to $\theta_t = 0.035$. A power law was found to fit the data points well, given by

$$\frac{L}{d} = \frac{0.16}{(1 - \theta/\theta_t)^2}. \quad (3.1)$$

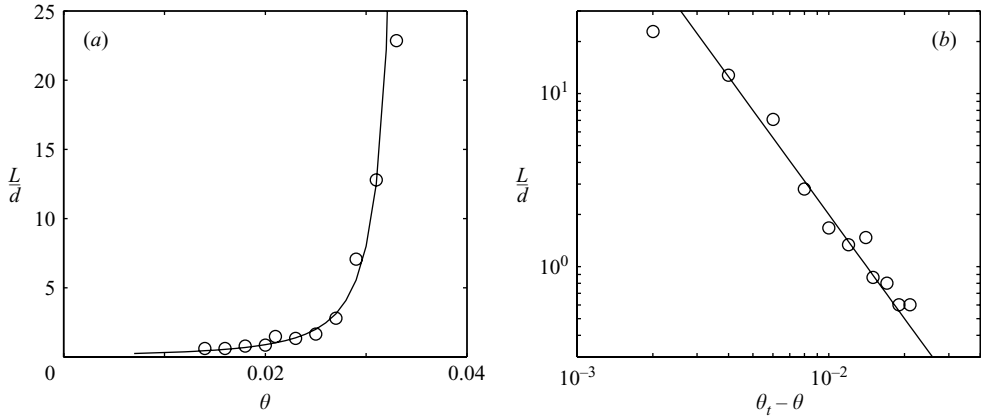


FIGURE 4. Mean distance travelled by the moving particle versus Shields number, (a) in linear scales and (b) in logarithmic scales (series 1). The solid lines correspond to the power law (3.1).

The threshold Shields number for mobile granular beds has received much attention for a long time and mechanistic models have been proposed, see the review by Buffington & Montgomery (1997). The difference that appears here between the threshold θ_{i0} for the first motion and that θ_i for continuous motion can be related to the phenomenon of ‘bed armouring’ (Chin, Melville & Raudkivi 1994), which leads to a decrease of the surface density of mobile particles over long times (Charru *et al.* 2004).

3.2. Trajectories, velocities and velocity distributions

As explained in the previous section, image analysis of all the experiments was performed for all series. The fundamental measure obtained directly from the images is the position of the particle as a function of time. With this measure, the trajectories of the beads can be analysed.

Figure 5 shows typical results of the bead trajectory for three values of the Shields number. Figure 5(a) shows the results obtained from the top view (x, y positions) and figure 5(b), shows the trajectories obtained from the side view (x, z positions). The motion of the bead is in all cases from left to right. In all cases the displacement in the streamwise direction (x -direction) is much more important than in the other two directions (y - or z -directions). For low values of the Shields number, for which the hydrodynamic force is slightly above the onset of motion, the trajectory of the bead appears to follow the geometry of the bed more closely. Hence, the particle rolls in nearly persistent contact with the substrate. Clearly, the periodicity observed in the trajectories for this case is indicative of the length scale of the roughness of the bed. Note that in figure 5(a) two traces are presented for the same nominal low value of the Shields number. In those particular experiments the particle passed through approximately the same position when first tracked (0, 0). It is interesting to observe that the two experiments show approximately the same trajectory for the first 5 mm ($\approx 3d$), but then take a different path. As the Shields number increases, the trajectory of the particle begins to depart from that dictated by the base and a few ‘jumps’ begin to be noticeable. The wavelength of the periodicity of the trajectories increases and the magnitude of the cross-streamwise displacement (y -direction) decreases. For higher values of the Shields number, the particle moves mainly in the x -direction and, as observed in the figure, exhibits longer flights. The inwards drift in the transverse

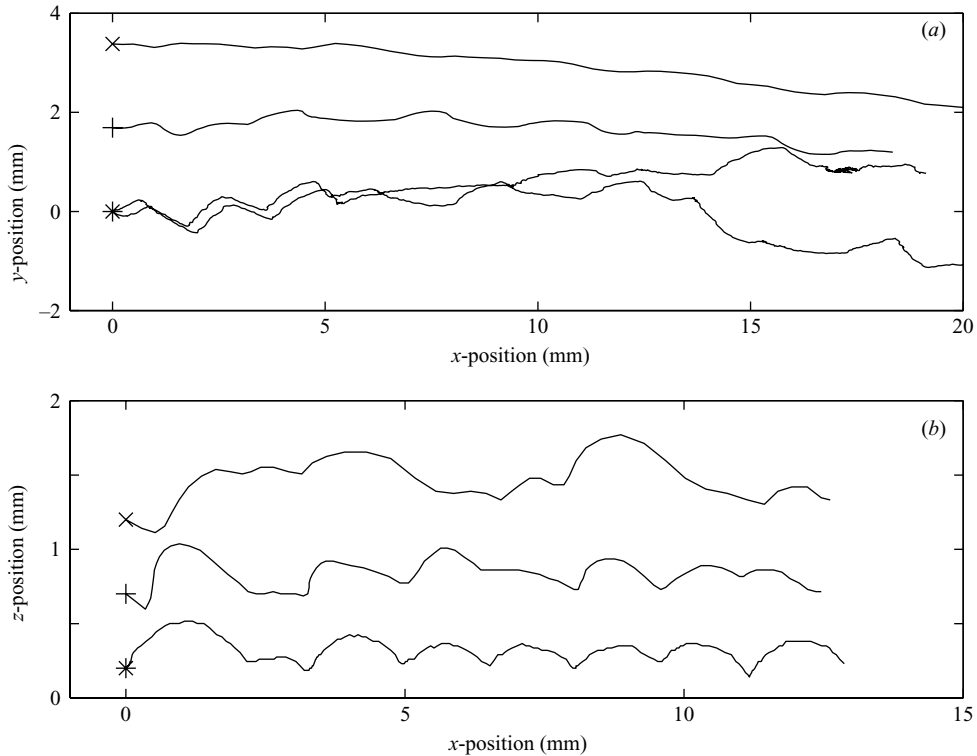


FIGURE 5. Typical particle trajectories from series 1, for three values of the Shields number: (a) x, y positions for $\theta = 0.07$ (*), 0.19 (+), 0.37 (\times); (b) x, z positions for $\theta = 0.09$ (*), 0.19 (+), 0.32 (\times). For clarity, the initial point is artificially displaced vertically. Note that the trajectories for $\theta = 0.19$ in (a) and (b) do not correspond to the same run, and that in (b) the scale on the vertical axis z is larger than on the horizontal one x .

y -direction is due to the secondary inertial flow discussed in §2. Correspondingly, the mean vertical position increases by $0.06d$ in the range $\theta = 0.09$ – 0.32 . Later in the paper, the power spectra of the particle motion will show two characteristic time scales of the motion, a shearing time scale and a settling time scale.

The particle velocity can be obtained from the position–time information obtained from image analysis. The instantaneous particle velocity was calculated using a central difference scheme. The x -direction velocity, $U(t)$, and y -direction velocity, $V(t)$, are shown on the left column of figure 6(a), for the same values of the Shields number as in figure 5(a). Clearly, the velocity traces are fluctuating in nature, in both directions. The streamwise velocity of the particle fluctuates around a mean value which increases with Shields number. Note that for the lowest Shields number ($\theta = 0.07$, upper trace) there are three points with negative streamwise velocity, which correspond to the sphere falling backwards into a trough. The transverse velocity also fluctuates around a slightly negative value corresponding to the inertial radial drift. A characteristic frequency of fluctuation can be readily discerned from the traces which will be analysed in §3.5. Along with the velocity traces, the normalized probability density functions (PDFs) of the velocities are shown on the right column of figure 6(b). The PDFs show that the velocity signals have a near-Gaussian distribution for the cases shown, with a slight skewness towards slower velocities for small Shields number and towards higher velocities as the Shields number increases. Note that the

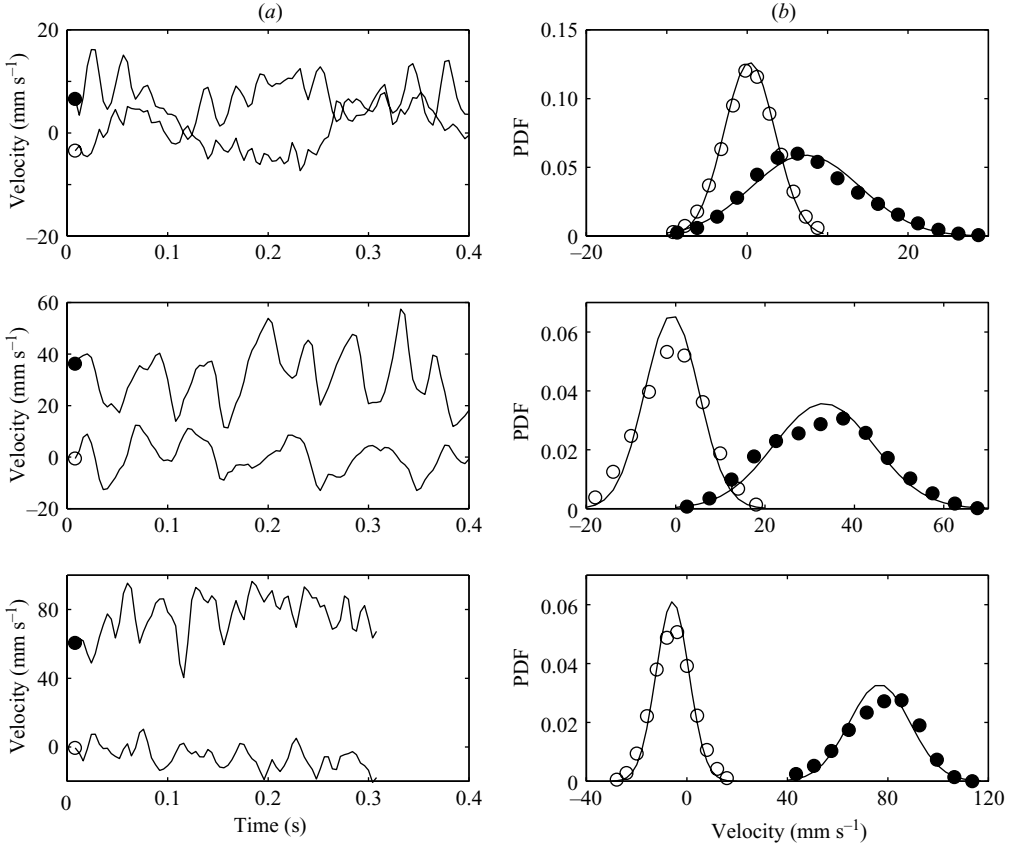


FIGURE 6. (a) Streamwise velocity $U(t)$ (●) and transverse velocity $V(t)$ (○) corresponding to the particles trajectories shown in figure 5(a). (b) The corresponding probability distribution functions and Gaussian curves. From top to bottom, Shields number is $\theta = 0.07, 0.19,$ and 0.37 .

Gaussian curves were calculated from the mean and variance of the velocity signals. Figure 7 shows the velocity signals obtained from the traces shown on figure 5(b), corresponding to the streamwise and vertical directions. Both components of the velocity fluctuate around a mean. The vertical velocity component, $W(t)$, fluctuates around a zero mean for all values of the Shields number. As in the previous case, changes in the structure of the traces can be readily noticed. At low values of the Shields number, the velocity fluctuations are a result of the interaction of the particle with the rough wall; as the strength of the shear increases, the particle may ‘fly’ after moving from a peak of the substrate. The evolution of the velocity with Shields number is discussed below. It may be noted from a comparison of figures 6 and 7 that the vertical velocity W is strongly correlated to the streamwise one (with a small delay), whereas the transverse velocity V is much less correlated.

3.3. Mean velocity

The mean value of streamwise velocity, U , was obtained for all the experiments performed in this investigation. Figure 8 shows the calculated value of U as a function of the flow shear rate, γ , for all the series. For one of the series, the error

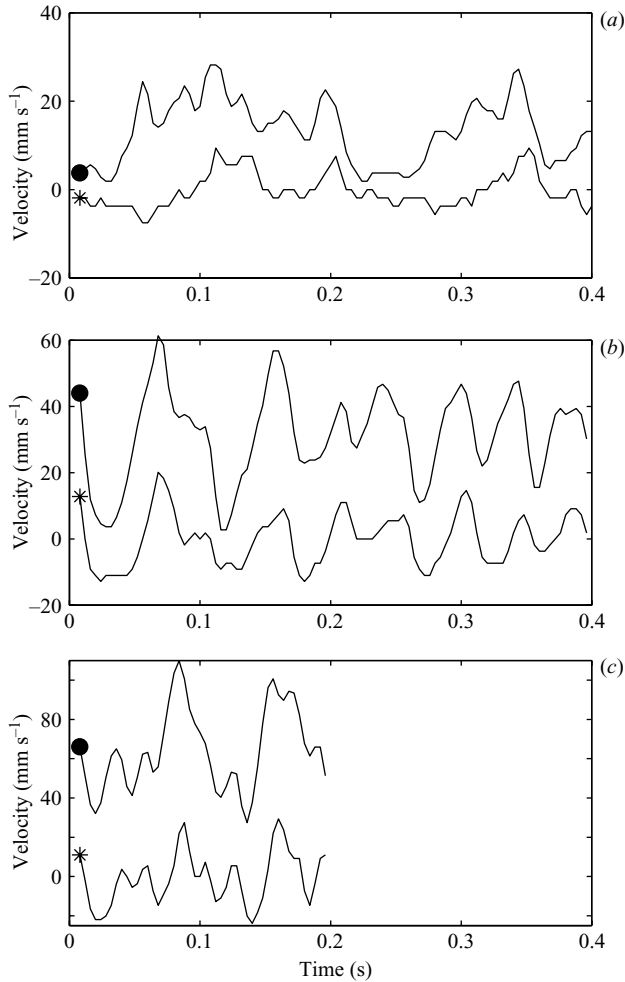


FIGURE 7. Streamwise velocity $U(t)$ (●) and vertical velocity $W(t)$ (*) corresponding to the particles trajectories shown in figure 5(b). Shields number is (a) $\theta = 0.09$, (b) $\theta = 0.19$, and (c) $\theta = 0.32$.

bars are shown. The estimated overall uncertainty of the velocity measurements is about 5%. For all cases shown, the mean particle velocity increases with shear rate. Also, for all cases, the particle moves only beyond a threshold shear rate, as discussed in §3.1, which is associated with a minimum non-zero velocity.

It is possible to normalize the measurements to collapse them into a single curve. Figure 9 shows the mean velocity normalized by the Stokes settling velocity, U/U_S , as a function of the dimensionless shear rate, or Shields number θ . Clearly, the velocity measurements presented in this manner are a function of the Shields number only, whatever the (small) particle Reynolds number. For $\theta < 0.17$, which corresponds to $U < U_S$, the normalized velocity appears to be a linear function of θ . In the insert which is a close-up of the measurements at low θ , the onset of particle motion can be clearly observed, at the threshold Shields number $\theta_t = 0.04$ with the threshold velocity $U_t/U_S \approx 0.1$. Above $\theta = 0.17$ the dimensionless velocity is higher than that given by the linear fit of the low- θ points.

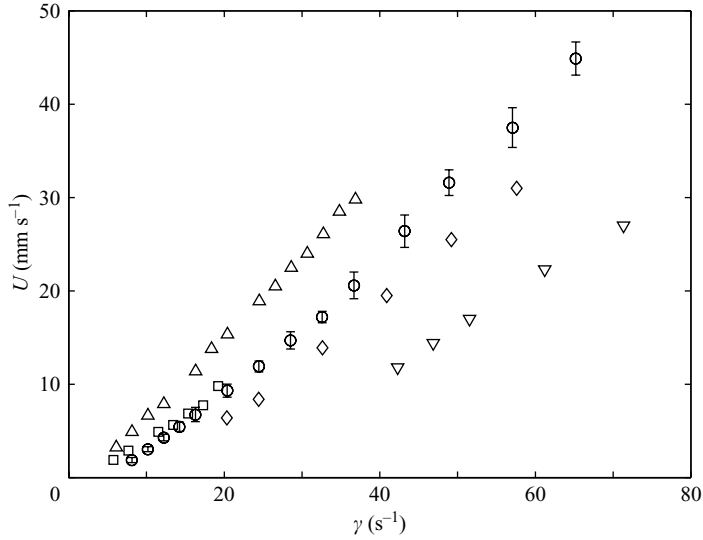


FIGURE 8. Streamwise particle velocity versus shear rate for all series (for symbols, see table 1). For series 1 (\circ) error bars show the scatter between the lowest and highest measured velocity.

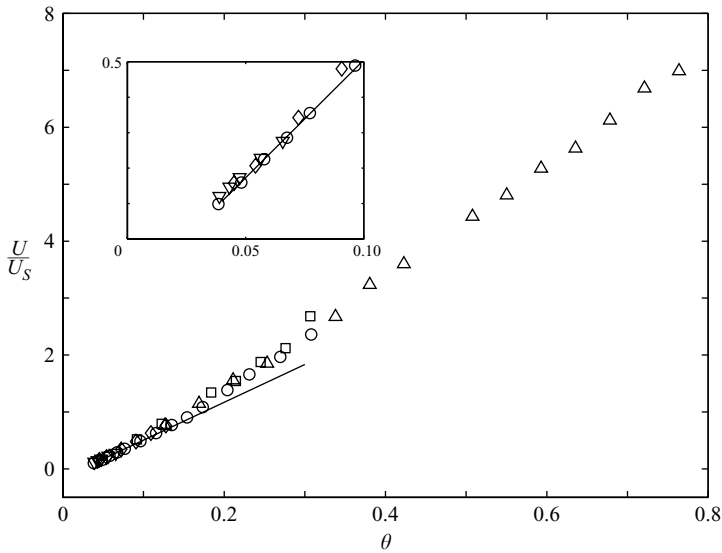


FIGURE 9. Normalized particle velocity U/U_s versus Shields number for all series, and magnification of the region near the origin. The straight line is a linear fit of the first points.

3.4. Velocity fluctuations

A measure of the fluctuating nature of the particle motion can be obtained from an analysis of the velocity traces. The standard deviations u' and v' of the particle velocity have been calculated for the streamwise and transverse directions. These are shown in figure 10 as a function of the Shields number for series 1, 4 and 5. Also, since a few visualization experiments were performed from a side view, some measurements

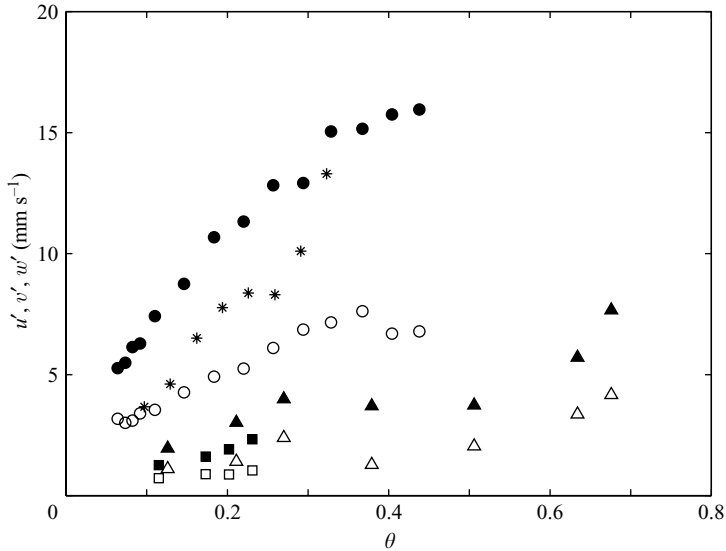


FIGURE 10. Streamwise velocity fluctuation u' (solid symbols) and transverse velocity fluctuation v' (open markers) versus shear rate for series 1, 4 and 5. The vertical fluctuation w' (stars) is shown for series 1 only.

of the vertical velocity standard deviation, w' , are shown. For all cases, the velocity fluctuations are found to increase with the strength of the imposed shear.

In a manner similar to that for the mean velocity, the measurements appear to collapse onto a single curve that depends only on the Shields number if they are normalized with the Stokes velocity, U_S . The normalized measurements are shown in figure 11 as a function of the Shields number. Although some scatter is present, the streamwise velocity fluctuation show a behaviour that can be fitted closely to

$$\frac{u'}{U_S} = 1.32\theta^{0.6}. \quad (3.2)$$

The transverse velocity fluctuations v' are found to follow the same power-law dependence with θ , but have a magnitude which is approximately half of that of the streamwise fluctuation:

$$v' = \frac{1}{2}u'. \quad (3.3)$$

The normalized vertical fluctuations w'/U_S are not shown in figure 11. Very few experiments were performed from the side view. Although the normalized vertical fluctuations do show a power-law behaviour similar to the other two directions, the scatter is larger and, therefore, a conclusive result cannot be given. In general the vertical fluctuations are smaller than the streamwise ones but larger than the transverse ones.

3.5. Particle velocity spectra

To further investigate the fluctuating nature of the particle motion over the rough substrate, the Fourier transform of the time-velocity traces was obtained, using the *spectrum* function from Matlab[®].

Figures 12 and 13 show some typical spectra of the streamwise velocity for three experimental series. Figure 12 shows the spectra for series 1 for which the high-speed

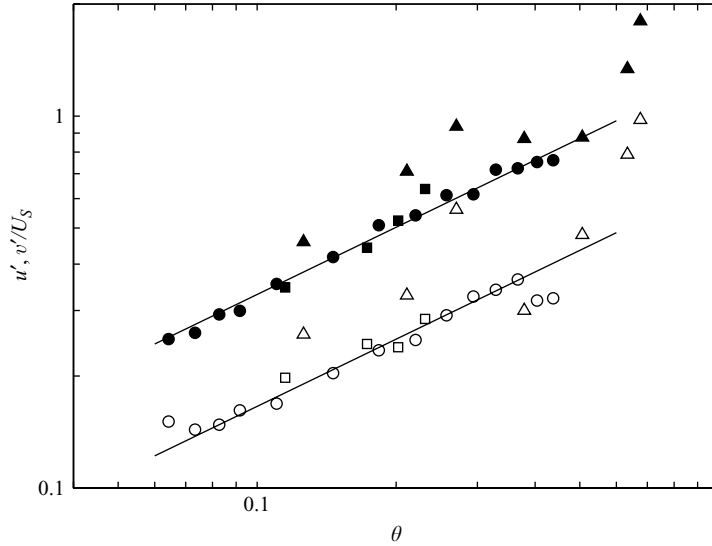


FIGURE 11. Normalized streamwise velocity fluctuation u' (solid symbols) and transverse velocity fluctuation v' (open symbols) versus Shields number, in logarithmic scales. The lines correspond to equations (3.2) and (3.3).

camera was used, allowing higher time resolution. These correspond to the velocity traces on figure 6 for the three values of the Shields number. From the figure, it is clear that the motion contains dominant frequencies, and that these evolve as the strength of the shear increases. Two characteristic frequencies are also shown on the plot: the ‘shear frequency’, U/d , (depicted by a star) and the ‘settling frequency’, U_S/d (depicted by a circle). Note that for a given experimental series, the shear frequency increases with the Shields number while the settling frequency is constant. For the lowest Shields number, for which $U < U_S$, the frequency of the highest peak corresponds to that of the shear frequency. This is an indication that the fluctuating motion of the particle is a result of the interaction with the wall, as the particle is dragged by the viscous shear over bed roughness. At the other extreme, for the highest Shields number shown, for which $U > U_S$, the frequency of the peak with maximum amplitude is closer to the settling frequency. For this case, it can be argued that the fluctuating motion is now dominated by the particle ‘jumps’ or small flights that occur after it passes over a peak of the rough substrate. For the intermediate value of the Shields number, which corresponds to $U \approx U_S$, two peaks with similar strengths can be discerned. The frequencies corresponding to the peaks are close to the two dominant frequencies; hence, for this case, the fluctuating motion results both from the interaction with the wall and the appearance of small flights. It must be noted that although the appearance of the peaks close to one characteristic frequency is clear on the figure, it may be less evident for other cases. Longer time series would be needed in order to obtain a better measure of the peak frequencies, and more generally better statistics of the fluctuating motion. Such long times series were not possible to obtain with the present setup.

Figure 13(a) shows the spectra for series 4 and figure 13(b) for series 5, along with the characteristic frequencies $1.1U/d$ and $0.5U_S/d$. These were found to be closer to the dominant peaks than the previously shown frequencies U/d and U_S/d . An analysis of the entire data set, for all series, indicated that those values gave a closer

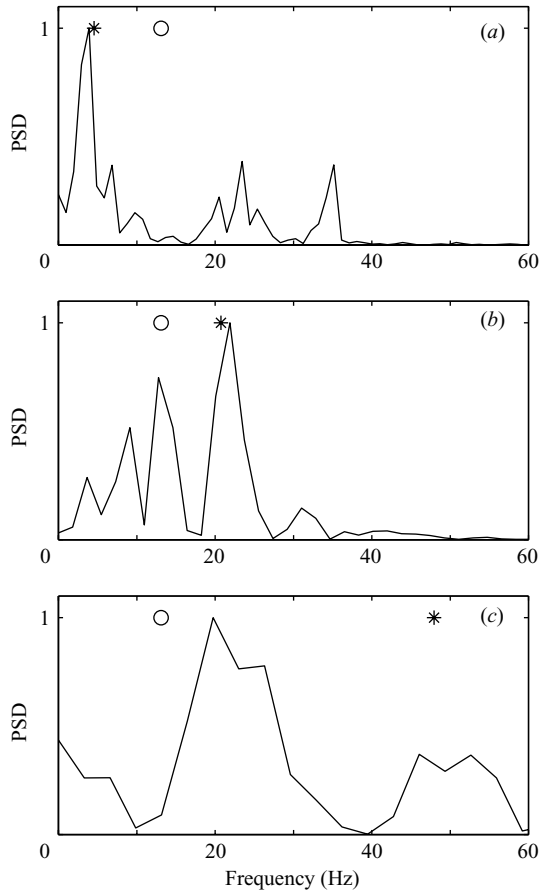


FIGURE 12. Power density spectra of the streamwise velocity corresponding to the particles trajectories shown in figure 5(a) (series 1, (a) (b) (c) $\theta = 0.07, 0.19$ and 0.37). The star (*) corresponds to the shear frequency U/d and the circle (\circ), to the settling frequency U_S/d .

correspondence to the peak frequencies. Figure 13 features the same behaviour as observed for series 1 (figure 12): for small Shields number, the dominant frequency is quite close to the shear frequency; as the Shields number is increased the dominant frequency evolves, reaching the settling frequency for the highest Shields numbers investigated here. Again, although the appearance of the dominant peaks close to the characteristic frequencies is clear in figure 13, the spectra from other experiments may not provide a conclusive result, which can be attributed to the short duration of the time series.

Finally, from the analysis of all the spectra obtained, it can be concluded that for small Shields number, $\theta < 0.2$, the dominant frequency is

$$n_1 \approx 1.1 \frac{U}{d}, \quad (3.4)$$

which indicates that the fluctuating motion is dominated by displacement of the particle over the bed geometry. For higher Shields number, another frequency arises in the spectra, which does not depend on the shear rate and scales with the settling

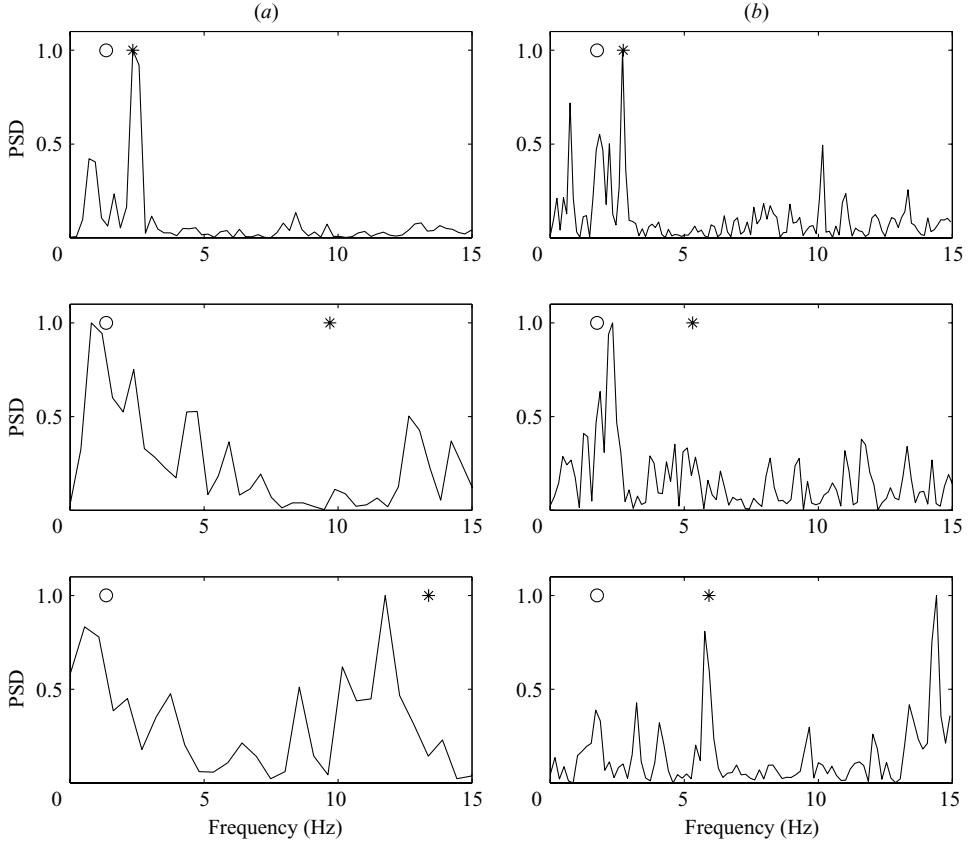


FIGURE 13. (a) Power density spectra of the streamwise velocity for three typical runs of series 4; from top to bottom, $\theta = 0.13, 0.38$ and 0.55 . The same for series 5 and $\theta = 0.12, 0.17$ and 0.20 . The star (*) corresponds to the shear frequency $1.1 U_s/d$ and the circle (\circ), to the settling frequency $0.5 U_s/d$.

frequency U_s/d . This frequency is in the range

$$0.5 U_s/d < n_2 < U_s/d, \quad (3.5)$$

and corresponds to the settling time of particles after small jumps from the top of the peaks of the rough substrate to the following trough.

4. Theory

The aim of this section is not to develop a new hydrodynamic model, but to propose a simple interpretation of our experiments within the framework of existing models developed for closely related situations. Simple and useful ideas to describe the motion of a particle near a rough wall in a shear flow were proposed by Bagnold (1973), of which a brief account is given in §4.1. This model introduces the notions of mean effective fluid velocity, drag coefficient near a wall and effective friction coefficient. A second model is then discussed, based on hydrodynamic calculations by Goldman *et al.* (1967*b*) for the related problem of the flow around a sphere near a smooth plane wall. These calculations and their use by Krishnan & Leighton (1995) in the case of

a rough particle touching a plane wall are presented in §4.2. This work is extended to a rough wall in §4.3, in order to account for the experiments reported above.

4.1. Bagnold's model

In his analysis of the fluctuating motion of a particle near a sand bed, Bagnold (1973) assumes that the mean horizontal force on the particle can be split into a fluid force corresponding to hydrodynamic interactions and a bed force corresponding to momentum transfer to the bed through collisions. A particle with mean velocity U is supposed to experience a mean effective fluid velocity u , so that the hydrodynamic force can be written as $C_D 3\pi\mu d(u - U)$ where $3\pi\mu d(u - U)$ is the Stokes drag force and C_D is an unknown drag coefficient of order one for viscous flow; this coefficient takes into account fluid inertia but also the vicinity of the wall and unsteadiness effects. The bed force can be written as a friction Coulomb force $\mu_f m'g$ where $m'g = (\rho_p - \rho)g\pi d^3/6$ is the immersed weight of the particle and μ_f is an 'effective' friction coefficient. This coefficient is expected to be different from the 'microscopic' friction coefficient at the contact point between the particle and the rough bed, since it accounts for the additional resistance due to the non-zero angle due to large roughnesses at contact. Then the equilibrium condition gives

$$\frac{U}{U_S} = 18 u_{eff} \theta - \frac{\mu_f}{C_D} \quad (4.1)$$

where U_S is the Stokes velocity (2.3), and $u_{eff} = u/(\gamma d)$ is a dimensionless effective fluid velocity. From the experiments reported above, the values of u_{eff} and μ_f/C_D can be determined from a linear fit of the data points in figure 9 near the threshold, giving

$$u_{eff0} = 0.37, \quad \frac{\mu_{f0}}{C_{D0}} = 0.16, \quad (4.2)$$

where the subscript '0' refers to the linear fit. In order to determine μ_{f0} and C_{D0} , and not just their ratio, another experiment is needed; Bagnold proposed using the friction coefficient he found in his experiments on the shearing of suspensions of spheres in a Couette flow (Bagnold 1954), which is $\mu_{f0} = 0.75$ for viscous flow. Hence the drag coefficient $C_{D0} = 4.7$.

Finally, of the three coefficients involved in Bagnold's model, the effective velocity u_{eff} but the ratio μ_f/C_D can be determined by direct velocity measurements and the friction coefficient μ_f has to be determined from a quite different experiment. It must be noted here that the validity of results on the shear properties of suspensions reported by Bagnold (1954) has recently been shown to be questionable (Hunt *et al.* 2002), and that a general theory for the friction coefficient is still an open problem for granular flows, see e.g. Midi (2004). Moreover the fact that only the ratio μ_f/C_D is directly measurable may signify that the decomposition between a fluid force and a bed force is questionable. An improved model is proposed below.

4.2. Particle on a smooth plane

As mentioned in the Introduction, the problem of the steady motion of a sphere near a plane wall, as sketched in figure 1(a), was solved by Goldman *et al.* (1967b) in the creeping flow limit. Since the Stokes equations and boundary conditions are linear, the motion of a sphere, with radius a and at distance h from the wall, may be solved separately in terms of three superposable contributions:

(i) a translational motion with velocity U in a fluid at rest far from the wall, corresponding to the hydrodynamic force and torque on the sphere

$$F_t = 6\pi\mu a U F_t^*, \quad T_t = 8\pi\mu a^2 U T_t^*, \quad (4.3)$$

where the dimensionless force F_t^* and torque T_t^* only depend on the dimensionless distance h/a ;

(ii) a rotational motion with angular velocity Ω in a fluid at rest far from the wall, corresponding to the hydrodynamic force and torque on the sphere

$$F_r = 6\pi\mu a^2 \Omega F_r^*, \quad T_r = 8\pi\mu a^3 \Omega T_r^* \quad (4.4)$$

(clockwise torques and angular velocities are positive, as in previous papers);

(iii) a shear flow γz past a fixed sphere, inducing the hydrodynamic force and torque

$$F_s = 6\pi\mu a(\gamma h) F_s^*, \quad T_s = 4\pi\mu a^3 \gamma T_s^*. \quad (4.5)$$

The starred dimensionless forces and torques appearing in the above equations only depend on the dimensionless distance h/a . Explicit expressions for these are given by Goldman *et al.* (1967*a, b*) in the two limits of a sphere far from the wall ($h \gg a$) and very close to the wall ($h - a \ll a$), see the following section. From the equilibrium conditions (zero net force and torque) the translational velocity $U/(\gamma a)$ and rotational velocity $\Omega/\frac{1}{2}\gamma$ of the free sphere are obtained as functions of the distance h/a .

Small inertia effects result in a lift force normal to the wall. This lift force was calculated by Cherukat & McLaughlin (1994) for a sphere translating and rotating close to the wall, and the limit of a sphere in contact with the wall was given by Krishnan & Leighton (1995) and King & Leighton (1997). In the latter two studies, these results were used to investigate the motion of a heavy rough sphere rolling on a smooth plane (figure 1*b*), whose centre is maintained at a distance $h > a$ from the wall by a typical roughness $h - a$ (this roughness is needed to resolve the particle motion because of the logarithmic singularity at the contact point for a smooth sphere). In addition to the hydrodynamic forces and torques (4.3)–(4.5), the problem now involves a contact force with tangential component F_c and normal component N . This normal component balances the sum of the immersed weight $m'g$ and the hydrodynamic lift force F_L . The equilibrium conditions become

$$N - m'g + F_L = 0, \quad (4.6a)$$

$$F_t + F_r + F_s - F_c = 0, \quad (4.6b)$$

$$T_t + T_r + T_s + a F_c = 0. \quad (4.6c)$$

Introducing a Coulomb friction force with friction coefficient μ_f , Krishnan & Leighton and King & Leighton considered the following three cases, corresponding to increasing shear rate: (i) rolling without sliding when $F_c < \mu_f N$, (ii) rolling and sliding when $F_c = \mu_f N$, and (iii) takeoff of the particle when the lift force overcomes the immersed weight. They calculated the particle velocity for the three regimes and found the predictions in agreement with their experiments.

4.3. Particle on a rough bed

Consider now a smooth particle moving on a rough bed made of loosely packed fixed particles, with diameter $h - a$ small compared to a , as sketched in figure 1(*c*). Because of the fixed small particles, the fluid velocity far from the bed is now $\gamma(z + \epsilon)$, where $z = 0$ now corresponds to the plane tangent to the top of the small particles, and ϵ is

an unknown length of order $h - a$. It may be expected that, as long as $(h - a) \ll a$, the particle velocity is still given by the equilibrium equations (4.6), with accuracy of order $(h - a)/a$.

In our experiments, the bed particles are identical to the moving particle as sketched in figure 1(d). In addition to the problem of the unknown length ϵ entering the far-field fluid velocity, the modelling must address the following features mentioned in the introduction: (i) the undefined ‘roughness length’ $(h - a)$, (ii) the mean slip velocity $(U - \Omega a)$, and the threshold shear rate (corresponding to the threshold Shields number $\theta_t = 0.04$).

The problem for the mean motion of the particle may be solved by considering that the hydrodynamic forces in (4.6) now are mean forces whose dependence on the mean velocities is still given by the expressions found by Goldman *et al.* (1967b), the distance h now being an unknown mean distance from the bed to be determined from the experiments. Hydrodynamic forces associated with unsteadiness and inertia are ignored here. Although the correction due to unsteadiness could be estimated from expressions given by Happel & Brenner (1965) for a smooth plane, this has not been attempted here. Ignoring the inertial lift force is consistent with the fact that the dimensionless mean velocities shown in figure 9 collapse onto the same curve, whatever the (small) particle Reynolds number. In addition, it is also consistent with the fact that, from Krishnan & Leighton (1995), takeoff would occur for Shields numbers such that $\theta Re_p = 5$, much higher than those investigated here.

The time-averaged momentum transfer through contacts with the bed, which may involve sliding and non-sliding stages at the contact point, is expected to reduce to a contact force with normal component N and tangential component F_c . As in Bagnold’s model, these components are assumed to follow the Coulomb relation $F_c = \mu_f N$ where μ_f is an effective friction coefficient, different from the microscopic friction coefficient. From a formal point of view, this coefficient arises from the time-averaging of the nonlinear conditions at the contact point (a succession of sliding and non-sliding stages). Note that the distinction between sliding and non-sliding stages is lost in the averaging procedure. Setting the equality $F_c = \mu_f N$ also accounts for the fact that particle motion requires the hydrodynamic force to be greater than some non-zero F_c , i.e. accounts for the existence of the threshold shear rate.

With these assumptions, the equilibrium conditions (4.6) together with equations (4.3)–(4.5) yields

$$U F_t^* + a\Omega F_r^* + \gamma h F_s^* - \mu_f U_S = 0, \quad (4.7)$$

$$U T_t^* + a\Omega T_r^* + \frac{1}{2}\gamma a T_s^* + \frac{3}{4}\mu_f U_S = 0, \quad (4.8)$$

where U_S is the Stokes velocity (2.3). On solving these equations, the particle velocity is found to have the same form as (4.1) with the dimensionless effective fluid velocity $u_{eff} = u/(\gamma d)$ and drag coefficient C_D given by

$$u_{eff} = \frac{1}{2} \frac{(h/a)F_s^* T_r^* - \frac{1}{2}F_r^* T_s^*}{F_r^* T_t^* - F_t^* T_r^*}, \quad (4.9a)$$

$$\frac{1}{C_D} = \frac{T_r^* + \frac{3}{4}F_r^*}{F_r^* T_t^* - F_t^* T_r^*}. \quad (4.9b)$$

Then, using the following expressions for the dimensionless forces and torques, valid for $h/a \gg 1$ (Goldman *et al.* 1967a):

$$F_t^* = -\left[1 - \frac{9}{16} \frac{a}{h}\right]^{-1}, \quad T_t^* = \frac{3}{32} \left(\frac{a}{h}\right)^4, \quad (4.10a)$$

$$F_r^* = \frac{1}{8} \left(\frac{a}{h}\right)^4, \quad T_r^* = -\left[1 + \frac{5}{16} \left(\frac{a}{h}\right)^4\right], \quad (4.10b)$$

$$F_s^* = 1 + \frac{9}{16} \frac{a}{h}, \quad T_s^* = 1 - \frac{3}{16} \left(\frac{a}{h}\right)^3, \quad (4.10c)$$

the distance h_0/a corresponding to the experimental effective fluid velocity u_{eff0} (4.2) can be found from (4.9a), hence the value of C_{D0} from (4.9b), and the friction coefficient from (4.2). These are found to be

$$\frac{h_0}{a} = 1.03, \quad C_{D0} = 2.4, \quad \mu_{f0} = 0.38. \quad (4.11)$$

These values are reasonable, with friction coefficient being half that in Bagnold's model. Note that h_0/a is not large, and consequently the above approximate expressions for the dimensionless forces and torques would not be entirely applicable. However, from table 2 in Goldman *et al.* (1967b), comparing the exact and approximate values of the velocity $U/\gamma a$ for given h/a shows that the relative difference is only 11% for a distance as small as $h/a = 1.04$. Alternatively, approximate expressions for small $(h-a)/a$ could also be used, as given by Goldman *et al.* (1967b) and corrected by Williams, Koch & Giddings (1992), or linear interpolations between the exact values given by Goldman *et al.* (1967b) and Chaoui & Feuillebois (2003). These expressions give values for h_0/a and μ_{f0} which are about 3% higher than those given by (4.11), as discussed in the Appendix; this difference of 3% is about the same as the uncertainty in h_0/a implied by an experimental uncertainty of 5% in u_{eff} and C_D .

From equations (4.7)–(4.8), the rotation velocity Ω can also be obtained. It is found that, with the values of h_0/a and μ_{f0} given by (4.11), Ω is slightly larger than U/a close to threshold, corresponding to a negative slip velocity $U - \Omega a \dagger$, and quickly decreases to an asymptotic value close to $0.5U/a$. However, since rotation velocities were not measured, no comparison is possible.

As seen in figure 9, the straight line corresponding to $h_0/a = 1.03$ and constant friction coefficient $\mu_{f0} = 0.38$ fits the data points only for $\theta < 0.17$, corresponding to $U < U_s$. Beyond this value, the above model has to be refined. Two ways may be envisaged, as follows. The first way consists of considering that as the shear rate is increased, the observed increase of the velocity fluctuations corresponds to increasingly stronger collisions of the particle with the bed. Then, the momentum transfer rate $\mu_{f0} m' g$ corresponding to the constant friction coefficient μ_{f0} has to be corrected by that due to the collisions. Assuming that the characteristic streamwise velocity

† It may be noted that for a particle on a smooth plane, a resisting (negative) contact force is necessarily associated with a positive sliding velocity. However, for the rough plane considered here, the distinction between sliding and non-sliding motion is lost when the mean motion of the particle is considered, as explained at the beginning of the section. The coexistence of a resisting contact force and a negative mean velocity can be seen in the simple two-dimensional example of a particle rolling over a bumpy plane of identical touching cylinders: without sliding at the contact point, the ratio $U/\Omega a$ is $3/\pi$, leading to the negative effective slip velocity $(1 - \pi/3)U$.

fluctuation, u' , corresponds to collisions with the bed, with characteristic frequency n , the additional momentum transfer per unit time is $mn u'$. However, this additional momentum transfer due to collisions increases the total momentum transfer, so that the resulting curve $U/U_S = f(\theta)$ would be below the straight line (4.1), contrary to the observations. In fact, the correction of the momentum transfer through collisions has to be abandoned for another reason: the striking experimental result that all data points in figure 9 fall onto a single curve $U/U_S = f(\theta)$, whatever the particle Reynolds number, indicates that inertia effects are not important for both the fluid and the particle. Thus introducing particle inertia in the modelling of the momentum transfer to the bed would be inconsistent.

The second way of improving the model is based on the observation that as the Shields number is increased, the particle loses contact with the bed, on the lee-side of the bed particles at first, and then experiences small jumps with a rise of its mean vertical position. Accordingly, the distance h/a given by (4.11) is no longer constant. For small Shields number, a linear increase of this distance with $\theta - \theta_t$ can be assumed:

$$\frac{h}{a} = \frac{h_0}{a} (1 + c(\theta - \theta_t)) \quad (4.12)$$

where c is a parameter to be determined from the experiments. Using (4.10) for the dimensionless forces and torques, the linearized effective fluid velocity (4.9a) and drag coefficient (4.9b) are found to be

$$u_{eff} = u_{eff0} (1 + 1.77 c(\theta - \theta_t)), \quad (4.13a)$$

$$C_D = C_{D0} (1 - 1.41 c(\theta - \theta_t)). \quad (4.13b)$$

As expected, increasing the shear stress increases the effective fluid velocity and decreases the drag coefficient.

The variation of the friction coefficient can be obtained by comparing the time the particle spends in contact with the bed and the characteristic duration of the velocity fluctuations, which is the sum of the contact time and the flying time. During contact the particle moves over a distance of order d so that the contact time can be estimated as d/U . The characteristic duration of the velocity fluctuations was found from the experiments to be approximately d/U_S for $\theta > 0.17$, corresponding to $U > U_S$. Thus, the fraction of time the particle spends in contact with the bed decreases proportionally to U_S/U , and the friction coefficient is reduced in the same proportion. Thus, when the particle flies, i.e. for $\theta > 0.17$ or $U > U_S$, the friction coefficient becomes

$$\mu_f = \mu_{f0} \frac{U_S}{U} = \frac{\mu_{f0}}{18 u_{eff0} \theta - \mu_{f0} / C_{D0}}. \quad (4.14)$$

Note that the above linearized laws for u_{eff} , C_D and μ_f have the advantage of introducing only one fitting parameter c . Inserting these laws into the velocity equation (4.1), the coefficient $c=0.4$ is found to fit the experimental points over the whole Shields number range, as shown in figure 14. In this figure curve (b) corresponds to constant $\mu_{f0}=0.38$, with distance h/a increasing from 1.03 to 1.35 in the range $\theta=0.04-0.8$. Thus, a relatively small increase of h/a (32%) increases the velocity by a factor two. The velocity u_{eff0} increases by a factor 1.5 and the drag coefficient is reduced by a factor 0.57. Curve (c) in figure 14 includes the variation of the friction coefficient according to (4.14), with the same $c=0.4$. It can be seen that, although the friction coefficient decreases by a factor 5 in the range $\theta=0.17-0.8$, the effect on the velocity is rather small.

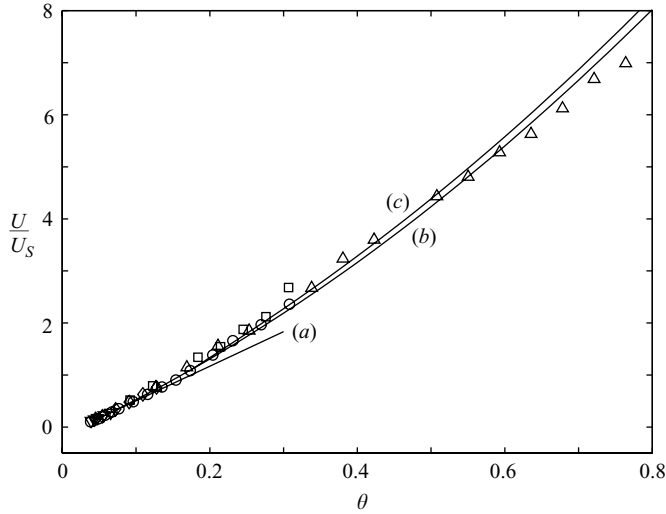


FIGURE 14. Normalized particle velocity U/U_S versus Shields number for all series. Continuous lines correspond to the model: straight line (a), equation (4.1) with constant effective distance h_0/a and friction coefficient μ_{f0} ; lower curve (b), varying h/a (equation (4.12)); upper curve (c), varying h/a and μ_f (equation (4.14)).

To summarize, it appears that the experimental results for the mean velocity can be accounted for by using the viscous forces calculated by Goldman *et al.* (1967a) and a Coulomb friction force for the momentum transfer to the bed. An effective friction coefficient, $\mu_{f0} = 0.38$, and an equivalent distance of the particle from the bed, $h_0/a = 1.03$, have been determined, so that the model fits the data points close to threshold. This model involves only two parameters, instead of three for Bagnold's model, and these two parameters have been determined from the velocity measurements without the need of other results from a different experiment. Far from threshold where the linear fit breaks down, allowing a small rise of the particle as the shear is increased fits the data over the explored Shields number range, although some discrepancy appears for the highest values of θ . The rise of the particle is associated with an increase in the effective fluid velocity and a decrease in the drag coefficient.

As a final remark, the problem of the spreading of a collection of particles deposited on a bed could be investigated with our experiments. The diffusion coefficients in the x - and y -directions could be determined from the distribution of particle displacements, as in Samson *et al.* (1998) for a particle on an inclined plane. It may be expected that these coefficients scale as the product of the characteristic velocity fluctuation u' or v' and the 'mean free path' found here. The study of this problem is postponed to future work.

5. Summary and discussion

Experiments have been reported on the motion of a single particle on a bed of fixed particles of the same diameter in a viscous shear flow. Five series of experiments have been performed with different fluid and particle physical properties: fluid viscosity, particle density and diameter. It was found that the mean velocities U , when scaled with the settling velocity U_S , all collapse on the same curve when plotted against the Shields number θ , whatever the particle Reynolds number. This collapse corresponds to the fact that the particle Reynolds number was less than ten, so that fluid inertia effects – as well as particle inertia effects – were small.

Velocity fluctuations have been measured in the three directions, featuring Gaussian distributions. The characteristic velocity fluctuations – root mean square values – when scaled with the settling velocity, collapse onto the same power law when plotted versus Shields number. Noticeably, the characteristic transverse fluctuation is half the streamwise one. Velocity spectra were more difficult to interpret due to the short time series. However, when the particle velocity is smaller than the settling velocity (Shields number $\theta < 0.17$), the dominant frequency was found to be $1.1 U/d$ showing that the fluctuating motion is dominated by the bed geometry. For higher velocity, another frequency arises in the spectra, which does not depend on the shear rate and scales with the settling frequency U_S/d . This frequency, which is between $0.5 U_S/d$ and U_S/d corresponds to small flights when the settling time in a trough is larger than the time spent by the particle above it.

In order to understand the mean streamwise velocity U , the model of Bagnold (1973) has been used first. Assuming for the friction coefficient $\mu_f = 0.75$ from Bagnold (1954), this model gives reasonable values for the effective fluid velocity $u_{eff} = u/(\gamma d) = 0.37$ and the drag coefficient $C_D = 4.7$. Then another model has been proposed, based on results of Goldman *et al.* (1967*b*) for the free motion of a sphere in a viscous shear flow parallel to a smooth plane. This model involves only two parameters, which were found by fitting the velocity measurements: the effective distance of the particle from the bed, or equivalent roughness, $h_0/a = 1.03$; and the friction coefficient, $\mu_{f0} = 0.38$. Note that this friction coefficient is half that used in Bagnold's model. For Shields number higher than 0.15, the measured velocities depart from the straight line corresponding to constant equivalent roughness and friction coefficient. An attempt was made to account for the greater velocity based on the observation that, as the shear is increased, the particle loses contact with the bed for longer and longer times, which raises its mean vertical position and reduces the momentum transfer to the bed. Use of the resulting shear-dependent distance h/a enables the model to fit well the data points, whereas the shear-dependent friction coefficient μ_f has little effect.

Our results for the mean streamwise velocity may be compared to those of King & Leighton (1997) for a rough particle on a smooth plane. The comparison is shown in figure 15, where the velocity is scaled with γd . Our data points are shown together with two theoretical curves presented by King & Leighton (1997) for their experimental data points. These curves correspond to the model (4.6) with $F_L = 0$, $\mu_f = 0.2$, and two values of the roughness: $(h - a)/a = 0.013$ and 0.026 . The horizontal lines for small θ corresponds to the case of pure rolling, and the curve for higher shear correspond to the case of rolling and sliding. It can be seen that for small shear, a particle on a rough bed travels slower than one rolling on a smooth plane, as expected. However, for higher shear, the particle on the rough bed travels faster, and the velocity difference increases with the shear (the rolling–sliding transition occurring at the crossing with our data points is fortuitous since this transition depends on the value of the friction coefficient). The fact that for high shear the particle on the rough bed travels faster than over a smooth plane is remarkable. This effect may be associated with the short flights as the particle loses contact with the bed, and the corresponding rise in its mean vertical position.

We would like to acknowledge D. Legendre for valuable discussions, X. Dubois for his work during the early stages of this study, and S. Cazin for technical assistance. Partial support for mutual visits between IMFT and IIM-UNAM was provided by the Secretaría Técnica de Intercambio Académico of CIC-UNAM and by the IIM-UNAM through its director, Dr. E. Sansores.

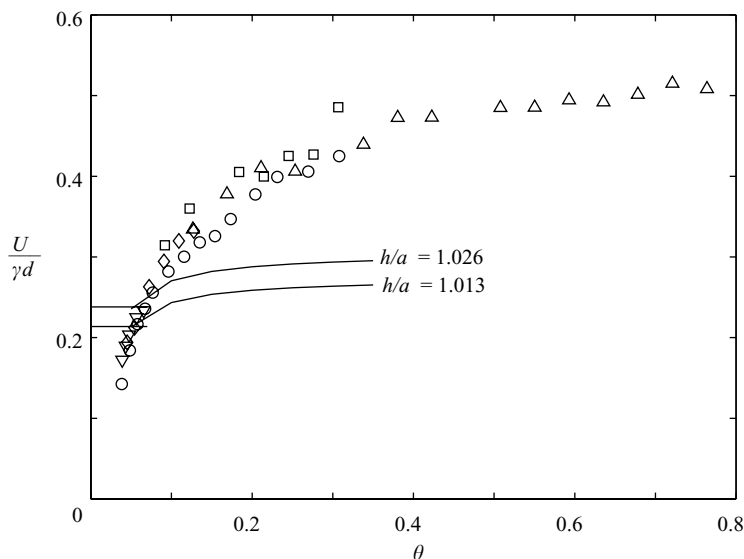


FIGURE 15. Same as figure 14 with $U/\gamma d$ instead of U/U_S . The curves are data of King & Leighton (1997).

Appendix. Alternative expressions for the forces and torques (4.10)

Since the distance h/a found from (4.10) is not large, the expressions for the forces and torques for small distance $(h-a)/a$ given by (Goldman *et al.* 1967*b*) and corrected by (Williams *et al.* 1992) could be used; these expressions, which involve a logarithmic dependence on $(h-a)/a$, give $h_0/a = 1.056$.

The precise interpolation formulae valid for all distances given by Chaoui & Feuillebois (2003) could also be used. Using the 38 terms given in their table 15, with 5 or 6 figures, one finds $h_0/a = 1.076$.

Another way is simply to interpolate the forces and torques from the exact values given by Goldman *et al.* (1967*b*) for $h/a = 1.0453$ and 1.1276 and by Chaoui & Feuillebois (2003) for $h/a = 1.1$. One finds $h_0/a = 1.068$ and $\mu_{f0} = n 0.42$.

Since the above values for h_0/a and μ_{f0} are close to those used in (4.11), and the improved model (with varying h/a) involves values of h/a up to 1.35, and the large distance expressions (4.10) give better results than the small distance expressions for h/a larger than 1.08, the values of h_0/a and μ_{f0} given by (4.11) have been used here.

REFERENCES

- ABBOT, J. E. & FRANCIS, J. R. D. 1977 Saltation and suspension trajectories of solid grains in a water stream. *Phil. Trans. R. Soc. Lond. A* **284**, 225–254.
- BAGNOLD, R. A. 1954 Experiments on a gravity-free dispersion of large solid spheres in a Newtonian fluid under shear. *Proc. R. Soc. Lond. A* **225**, 49–63.
- BAGNOLD, R. A. 1973 The nature of saltation and of ‘bed-load’ transport in water. *Proc. R. Soc. Lond. A* **332**, 473–504.
- BUFFINGTON, J. M. & MONTGOMERY, D. R. 1997 A systematic analysis of eight decades of incipient motion studies, with special reference to gravel-bedded rivers. *Water Resour. Res.* **33**, 1993–2029.
- CHAOUI, M. & FEUILLEBOIS, F. 2003 Creeping flow around a sphere in a shear flow close to a wall. *Q. J. Mech. Appl. Maths* **56**, 381–410.

- CHARRU, F., MOULLERON-ARNOULD, H. & EIFF, O. 2004 Erosion and deposition of particles on a bed sheared by a viscous flow. *J. Fluid Mech.* **519**, 55–80.
- CHERUKAT, P. & McLAUGHLIN, J. B. 1994 The inertial lift on a rigid sphere in a linear shear flow field near a flat wall. *J. Fluid Mech.* **263**, 1–18.
- CHIN, C. O., MELVILLE, B. W. & RAUDKIVI, A. J. 1994 Streambed armoring. *J. Hydraul. Engng* **120**, 899–918.
- FRANCIS, J. R. D. 1973 Experiments on the motion of solitary grains along the bed of a water stream. *Proc. R. Soc. Lond. A* **332**, 443–471.
- GOLDMAN, A. J., COX, R. G. & BRENNER, H. 1967*a* Slow viscous motion of a sphere parallel to a plane wall - I Motion through a quiescent fluid. *Chem. Engng Sci.* **22**, 637–651.
- GOLDMAN, A. J., COX, R. G. & BRENNER, H. 1967*b* Slow viscous motion of a sphere parallel to a plane wall - II Couette flow. *Chem. Engng Sci.* **22**, 653–660.
- HAPPEL, J. & BRENNER, H. 1965 *Low Reynolds Number Hydrodynamics*. Prentice Hall.
- HUNT, M. L., ZENIT, R., CAMPBELL, C. S. & BRENNEN, C. E. 2002 Revisiting the 1954 suspension experiments of R. A. Bagnold. *J. Fluid Mech.* **452**, 1–24.
- KING, M. R. & LEIGHTON, D. T. 1997 Measurement of the inertial lift on a moving sphere in contact with a plane wall in a shear flow. *Phys. Fluids* **9**, 1248–1255.
- KRISHNAN, G. P. & LEIGHTON, D. T. 1995 Inertial lift on a moving sphere in contact with a plane wall in a shear flow. *Phys. Fluids* **7**, 2538–2545.
- MIDI, G. D. R. 2004 On dense granular flows. *Eur. Phys. J. E* **14**, 341–365.
- O'NEILL, M. E. 1968 A sphere in contact with a plane wall in a slow linear shear flow. *Chem. Engng Sci.* **23**, 1293–1298.
- QUARTIER, L., ANDREOTTI, B., DOUADY, S. & DAERR, A. 2000 Dynamics of a grain on a sandpile model. *Phys. Rev. E* **62**, 106–114.
- RIGUIDEL, F.-X., JULLIEN, R., RISTOW, G. H., HANSEN, A. & BIDEAU, D. 1994 Behaviour of a sphere on a rough inclined plane. *J. Phys. Paris I* **4**, 261–272.
- SAMSON, L., IPPOLITO, I., BATROUNI, G. G. & LEMAITRE, J. 1998 Diffusive properties of motion on a bumpy plane. *Eur. Phys. J. B* **3**, 377–385.
- WILLIAMS, P. S., KOCH, T. & GIDDINGS, J. C. 1992 Characterization of near-wall hydrodynamic lift forces using sedimentation field-flow fractionation. *Chem. Engng Sci.* **111**, 121–127.
- ZHAO, Y., GALVIN, K.P. & DAVIS, R. H. 2002 Motion of a sphere down a rough plane in a viscous fluid. *Intl J. Multiphase Flow* **28**, 1787–1800.